THE JOURNAL OF PHYSICAL CHEMISTRY B

Article

pubs.acs.org/JPCB

Trigonal 1,3,4-Oxadiazole-Based Blue Emitting Liquid Crystals and Gels

Deepak D. Prabhu, N. S. Saleesh Kumar, Aneesh P. Sivadas, Shinto Varghese, and Suresh Das*

Photosciences and Photonics Section, Chemical Sciences and Technology Division, National Institute for Interdisciplinary Science and Technology (NIIST) and Network of Institutes for Solar Energy, CSIR, Trivandrum 695 019, India

ABSTRACT: Star-shaped molecules consisting of a 1,3,4-oxadiazole core derivatized with alkoxy-substituted phenyl ethynylenes, **FD12** (dodecyl) and **FD16** (hexadecyl) were synthesized. These molecules exhibited enantiotropic columnar mesophases over a wide temperature range, with the liquid crystalline phases exhibiting strong blue fluorescence. On cooling, **FD12** transformed into a transparent glass at room temperature wherein the liquid crystalline texture was retained. The glassy film remained stable over a period of one year and exhibited blue luminescence with an absolute quantum yield of 26%. The oxadiazole derivatives formed stable luminescent gels in decane and study of their morphology by scanning electron microscopy (SEM) and transmission electron microscopy (TEM) indicated formation of interlocked network of self-assembled fibers. X-ray diffraction (XRD) analysis of the xerogel of these derivatives indicated oblique columnar ordering of the molecules within the fibers. The length of the alkyl substituent was observed to have a significant effect on the absorption and fluorescence properties of the gels, which was attributable to the role of the alkyl substituents in controlling the nature of the molecular packing within the self -assembled fibers of the gels.

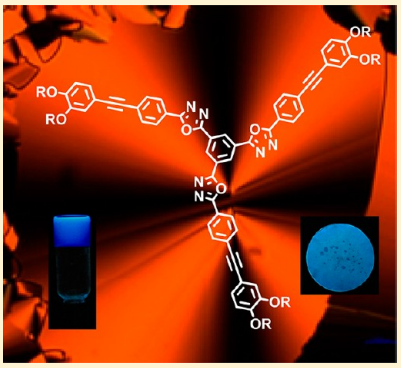

INTRODUCTION

Columnar liquid crystals are a class of soft materials which have attracted special attention because of their ability to form highly ordered superstructures.[1] The arrangement of π-conjugated materials into columnar stacks in such materials imparts them with unique functional properties such as the ability to efficiently conduct charge and energy in a highly anisotropic manner, making them useful materials for a variety of organic electronic and electro-optic devices.[2] In recent years there has been an increasing focus on the design of columnar liquid crystals exhibiting high degree of luminescence in their solid and liquid crystalline states because of their utility in display devices and organic light emitting diodes.[3] Design of such materials provides an interesting challenge, since the very intermolecular interactions which are essential for bringing about the self-assembly of molecules into columnar stacks can be detrimental to their luminescence efficiency. For example, $\pi-\pi$-interactions between neighboring molecules which can help in stabilizing columnar mesophases can lead to drastic reduction in the fluorescence efficiency of the molecules.[4,5] As a result most columnar liquid crystals exhibit weak fluorescence. Design of luminescent columnar liquid crystals will therefore require both proper choice of the chromophore as well as fine control of the self-assembly of the molecules. Geert's and co-workers have recently reported on highly fluorescent pyrene-based columnar liquid crystals, wherein the high luminescence efficiency in the solid state of these materials was ascribed to rotated chromophores, leading to minimal $\pi-\pi$ interaction between the neighboring molecules.[6] Suppression of π-stacking resulting in luminescent columnar liquid crystals was also reported in triazolotriazine derived molecules.[7]

We had earlier reported on a novel class of star shaped oxadiazole derivatives exhibiting columnar mesophases.[2a] 1,3,4-Oxadiazoles were incorporated in the core of the discotic molecules in view of their excellent electron transporting and luminescent properties as well as their ability to undergo efficient π-stacking.[8] Although in solutions the molecules inherently exhibited strong blue fluorescence, the columnar liquid crystals derived from these materials exhibited green fluorescence as a result of strong π-stacking interaction between neighboring molecules leading to the formation of fluorescent aggregates. In view of the significant interest in development of blue light emitting materials for applications in electro-optic and electroluminescent devices,[9] we have attempted to fine-tune the structure and self-assembly of this class of materials to obtain the desired emission. Here we report on the design and study of two new oxadiazole-based columnar liquid crystals (**FD12** and **FD16**) wherein the conjugation between the alkoxyphenyl donor substituent and the oxadiazole acceptor substituent was diminished by changing the linker group from vinyl to ethynyl (Chart 1).

These materials exhibited blue emission with high efficiency both in solution as well as in their liquid crystalline phase. Both these molecules exhibited enantiotropic columnar mesophases over a very wide range of temperature, among which **FD12** transformed into a transparent glass at room temperature wherein the liquid crystalline order was retained. The glassy films remained stable over a period of one year and exhibited

Received: June 1, 2012
Revised: October 6, 2012
Published: October 9, 2012

Chart 1

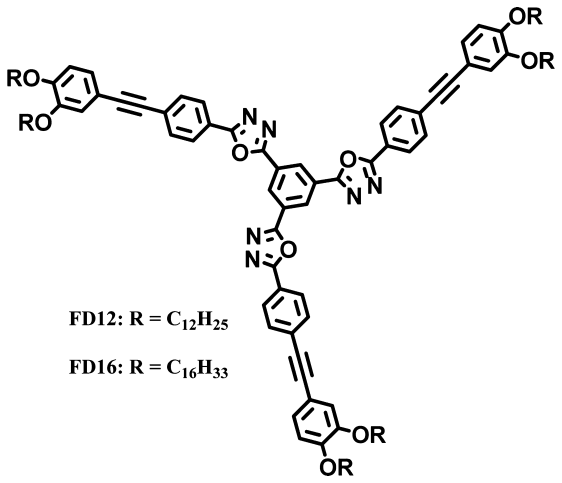

blue luminescence with an absolute efficiency of 26%. The ability of these molecules to gel nonpolar solvents such as decane has also been investigated. The gels thus formed exhibited blue to bluish-green luminescence. Gelation of the solvents was observed to be brought about by formation of a self-assembled fibrillar network wherein the molecules retained their columnar arrangement. These aspects as well as the detailed study on the effect of molecular structure and self-assembly on the photophysical properties of the molecules in their solution, liquid crystalline phase, gels, and aggregated state are described herein.

EXPERIMENTAL SECTION

Instrumentation. The solvents and the reagents were dried and purified by standard methods prior to use. Melting points were determined with a Mel-Temp-II melting point apparatus and are uncorrected. FT-IR spectra were recorded on a Shimadzu IR Prestige-21 Fourier Transform Infrared Spectrophotometer. ^{1}H (300 and 500 MHz) and ^{13}C NMR (125 MHz) spectral analysis were performed on a Bruker Avance DPX spectrometer with TMS as internal standard. MALDI−TOF mass spectrometry was conducted on a Perspective Biosystems Voyager DE PRO MALDI−TOF mass spectrometer using α-cyano-4-hydroxy cinnamic acid as the matrix. Electronic absorption spectra were recorded on a Shimadzu UV-3101 PC NIR scanning spectrophotometer and emission spectra were recorded on a SPEX-Fluorolog FL-1039 spectrofluorimeter. Optical absorption measurements were carried out using 1 mm or 10 mm cuvettes with a thermistor directly attached to the wall of the cuvette holder for controlling the temperature. Fluorescence measurements were carried out using 1 mm cuvette in a front face setup. Fluorescence quantum yields in solution were measured using quinine sulfate in 0.1 M H_2SO_4 (ϕ_F = 0.54) as reference. Fluorescence lifetimes were measured using IBH (FluoroCube) time-correlated picoseconds single photon counting (TCSPC) system. Solutions were excited with a pulsed diode laser (<100 ps pulse duration) at a wavelength of 375 nm (NanoLED-11) with a repetition rate of 1 MHz. The detection system consisted of a microchannel plate photomultiplier (5000U-09B, Hamamatsu) with a 38.6 ps response time coupled to a monochromator (5000 M) and TCSPC electronics [Data station Hub including Hub-NL, NanoLED controller and preinstalled fluorescence Measurement and Analysis Studio (FMAS) Software]. The fluorescence lifetime values were obtained using DAS6 decay analysis software. Absolute quantum yield in the liquid crystalline glassy film as well as in the gel state was measured using a calibrated integrating sphere in a SPEX fluorolog FL-1039 fluorimeter. For scanning electron microscopic (SEM) measurements, samples were drop cast and air-dried on flat surface of cylindrical brass stubs and subjected to thin gold coating using JEOL JFC-1200 fine coater. The probe was inserted into JEOL JSM-5600 LV scanning electron microscope for taking photographs. TEM measurements were carried out in JEOL 100 kV HRTEM. The samples were prepared by drop casting 25 μL of 5 × 10^{-5} M onto a carbon coated copper grid and solvent was allowed to evaporate under vacuum. Liquid crystalline phase transitions were observed using a Leica DFC 490 polarized light optical microscope, equipped with a Mettler TOLEDO FP82HT (Temperature programmer) heating and freezing stage. Differential scanning calorimetry was performed using a Perkin-Elmer Pyris 6 DSC instrument in sealed aluminum pans under nitrogen flow, at a heat/cooling rate of 5 °C/min. X-ray diffraction studies of xerogel was carried out on samples coated in glass slide and measurements were recorded on a Phillips diffractometer using Ni-filtered Cu Kα radiation (λ = 1.5418 Å). Details of the setup for the XRD studies carried out at CSMR, Bangalore, using samples filled using Lindemann capillaries, are given elsewhere.[10] The apparatus essentially involved a high-resolution X-ray powder diffractometer (PANalytical X'Pert PRO) equipped with a high-resolution fast detector, PIXCEL.

Synthesis. *General Procedure for the Synthesis of 1,2-Bis(alkoxy)benzene **1a** and **1b**.* Catechol (1 equiv), alkyl bromide (4 equiv), and K_2CO_3 (7 equiv) were dissolved in 30 mL of degassed DMF and were stirred at 80 °C for 24 h. The reaction mixture was then poured into ice cold water. The precipitate formed was filtered, washed with water, and dried. The crude product was further purified by column chromatography using silica gel (100−200 mesh) as the stationary phase and hexane as the mobile phase.

*1,2-Bis(dodecyloxy)benzene (**1a**).* This was obtained in 85% yield as a colorless amorphous solid; mp: 43−44 °C. ^{1}H NMR (300 MHz, $CDCl_3$): δ 6.88 (s, 4H), 3.96−4.00 (t, 4H), 1.78−1.85 (m, 4H), 1.26−1.47 (m, 36H), 0.85−0.90 (t, 6H) ppm. ^{13}C NMR (125 MHz, $CDCl_3$): 149.25, 121.0, 114.14, 69.29, 31.93, 29.72, 29.65, 29.45, 29.37, 26.06, 22.69, 14.12 ppm. IR (KBr) ν_{max}: 2951, 2914, 2850, 1587, 1508, 1461, 1455, 1390, 1257, 1220, 1122, 997, 732 cm^{-1}.

*1,2-Bis(hexadecyloxy)benzene (**1b**).* This was obtained in 84% yield as a colorless amorphous solid; mp: 55−56 °C. ^{1}H NMR (300 MHz, $CDCl_3$): δ 6.88 (s, 4H), 3.96−4.00 (t, 4H), 1.78−1.85 (m, 4H), 1.26−1.47 (m, 52H), 0.85−0.90 (t, 6H) ppm. ^{13}C NMR (125 MHz, $CDCl_3$): 149.25, 121.0, 114.14, 69.29, 31.93, 29.72, 29.65, 29.45, 29.37, 26.06, 22.69, 14.12 ppm. IR (KBr) ν_{max}: 2953, 2916, 2846, 1593, 1508, 1465, 1452, 1390, 1257, 1220, 1122, 997, 732 cm^{-1}.

*General Procedure for the Synthesis of 1,2-Bis(alkoxy)-4-iodobenzene, **2a** and **2b**.* 1,2-Bis(alkoxy)benzene (1 equiv) and *N*-iodosuccinimide (1.1 equiv) were dissolved in 20 mL of acetonitrile (ACN), to which 5 drops of trifluoroacetic acid was added, and the mixture was stirred for 6 h at room temperature. The reaction mixture was then extracted with dichloromethane and the organic layer was washed thoroughly with sodium thiosulphate solution and dried over anhydrous sodium sulfate. Excess solvent was removed under reduced pressure, and the

dx.doi.org/10.1021/jp305349h | J. Phys. Chem. B 2012, 116, 13071−13080

crude product was further purified by column chromatography using silica gel (100−200 mesh) as the stationary phase and 5% EtOAc: hexane as the mobile phase.

*1,2-Bis(dodecyloxy)-4-iodobenzene (**2a**).* This was obtained in 87% as a colorless amorphous solid; mp: 55−56 °C. ^{1}H NMR (300 MHz, $CDCl_3$): δ 7.16−7.19 (d, J = 8.4 Hz, 1H), 7.12 (s, 1H), 6.60−6.62 (d, J = 8.4 Hz, 1H), 3.92−3.96 (t, 4H), 1.78−1.85 (m, 4H), 1.26−1.47 (m, 36H), 0.85−0.90 (t, 6H) ppm. ^{13}C NMR (125 MHz, $CDCl_3$): 150.14, 149.78, 149.25, 129.80, 123.79, 122.68, 115.73, 95.96, 82.51, 69.43, 69.36, 31.94, 29.72, 29.62, 29.38, 29.18, 29.05, 25.98, 22.70, 14.12 ppm. IR (KBr ν_{max}: 2950, 2922, 2841, 1590, 1508, 1461, 1391, 1254, 1131, 1070, 993, 840, 800, 721 cm^{-1}.

*1,2-Bis(hexadecyloxy)-4-iodobenzene (**2b**).* This was obtained in 90% yield as a colorless amorphous solid; mp: 60−61 °C. ^{1}H NMR (300 MHz, $CDCl_3$): δ 7.16−7.19 (d, J = 8.4 Hz, 1H), 7.12 (s, 1H), 6.60−6.62 (d, J = 8.4 Hz, 1H), 3.92−3.96 (t, 4H), 1.78−1.85 (m, 4H), 1.26−1.47 (m, 52H), 0.85−0.90 (t, 6H) ppm. ^{13}C NMR (125 MHz, $CDCl_3$): 150.14, 149.78, 149.25, 129.80, 123.79, 122.68, 115.73, 95.96, 82.51, 69.43, 69.36, 31.94, 29.72, 29.62, 29.38, 29.18, 29.05, 25.98, 22.70, 14.12 ppm. IR (KBr) ν_{max}: 2954, 2918, 2846, 1581, 1502, 1465, 1394, 1257, 1136, 1070, 993, 840, 800, 721 cm^{-1}.

*General Procedure for the Synthesis of 4-((3,4-Bis(alkoxy)-phenyl)ethynyl)benzonitrile, **3a** and **3b**.* To a 100 mL two necked round-bottom flask kept under argon atmosphere were added 1,2-Bis(alkoxy)-4-iodobenzene (1.1 equiv), 4-ethynyl-benzonitrile (1 equiv), and a catalytic amount of palladium(II) chloride, CuI, and PPh_3 to 15 mL of degassed THF. To this was added 10 mL of degassed diisopropyl amine (DIPA) and the mixture stirred at room temperature for 12 h. The reaction mixture was then passed through a Celite column and the crude product was further purified by column chromatography using silica gel (100−200 mesh) as the stationary phase and 5% EtOAc: hexane as the mobile phase.

*4-((3,4-bis(dodecyloxy)phenyl)ethynyl)benzonitrile (**3a**).* This was obtained in 82% yield; mp: 85−86 °C. ^{1}H NMR (300 MHz, $CDCl_3$): δ 7.61−7.63 (d, J = 7.8 Hz, 2H), 7.56−7.59 (d, J = 8.1 Hz, 2H), 7.11−7.14 (d, J = 8.1 Hz, 2H), 7.05 (s, 1H), 6.84−6.87 (d, J = 8.1 Hz, 1H), 3.96−4.00 (t, 4H), 1.78−1.85 (m, 4H), 1.26−1.47 (m, 36H), 0.85−0.90 (t, 6H) ppm. ^{13}C NMR (125 MHz, $CDCl_3$): 150.46, 148.81, 132.01, 131.84, 125.40, 118.63, 116.69, 114.11, 113.13, 111.01, 94.46, 86.39, 69.33, 69.13, 31.93, 29.71, 29.63, 29.40, 29.37, 29.20, 29.15, 26.01, 22.69, 14.11 ppm. IR (KBr) ν_{max}: 2953, 2916, 2848, 2227, 2196, 1589, 1517, 1467, 1417, 1392, 1330, 1257, 1274, 1226, 1118, 1143, 1068, 995, 835, 810, 721, 557 cm^{-1}.

*4-((3, 4- bis(hexadecyloxy)phenyl)ethynyl)benzonitrile (**3b**).* This was obtained in 84% yield; mp: 91−92 °C. ^{1}H NMR (300 MHz, $CDCl_3$): δ 7.61−7.63 (d, J = 7.8 Hz, 2H), 7.56−7.59 (d, J = 8.1 Hz, 2H), 7.11−7.14 (d, J = 8.1 Hz, 2H), 7.05 (s, 1H), 6.84−6.87 (d, J = 8.1 Hz, 1H), 3.96−4.00 (t, 4H), 1.78−1.85 (m, 4H), 1.26−1.47 (m, 52H), 0.85−0.90 (t, 6H) ppm. ^{13}C NMR (125 MHz, $CDCl_3$): 150.46, 148.81, 132.01, 131.84, 125.40, 118.63, 116.69, 114.11, 113.13, 111.01, 94.46, 86.39, 69.33, 69.13, 31.93, 29.71, 29.63, 29.40, 29.37, 29.20, 29.15, 26.01, 22.69, 14.11 ppm. IR (KBr) ν_{max}: 2953, 2916, 2848, 2227, 2196, 1589, 1517, 1467, 1417, 1392, 1330, 1257, 1274, 1226, 1118, 1143, 1068, 995, 835, 810, 721, 557 cm^{-1}.

*General Procedure for the Synthesis of 5-(4-((3,4-Bis-(alkoxy)phenyl)ethynyl)phenyl)-2H-tetrazole, **4a** and **4b**.* In 25 mL of dry degassed DMF were dissolved 4-((3,4-bis(alkoxy)phenyl)ethynyl)benzonitrile (1 equiv), NaN_3 (2 equiv), and NH_4Cl (2 equiv), and the reaction was stirred at 100 °C for 12 h. The reaction mixture was then poured into ice cold water and neutralized with 50 mL of 10% HCl. The precipitate formed was then filtered, washed with water and dried. The crude product was then purified by column chromatography using silica gel (100−200 mesh) as the stationary phase and THF as the mobile phase.

*5-(4-((3,4-Bis(dodecyloxy)phenyl)ethynyl)phenyl)-2H-tetrazole (**4a**).* This was obtained in 85% yield as a colorless amorphous solid; mp: 121−123 °C. ^{1}H NMR (500 MHz, *d*-DMSO): δ 8.07−8.09 (d, J = 8 Hz, 2H), 7.64−7.66 (d, J = 8.0 Hz, 2H), 7.09−7.11 (d, J = 8.5 Hz, 1H), 7.05 (s, 1H), 6.89−6.90 (d, J = 8.0 Hz, 1H), 3.96−4.00 (t, 4H), 1.78−1.85 (m, 4H), 1.26−1.47 (m, 36H), 0.85−0.90 (t, 6H) ppm. ^{13}C NMR (125 MHz, *d*-DMSO): 154.95, 153.35, 137.19, 132.49, 130.59, 130.23, 121.45, 118.95, 118.62, 97.44, 92.29, 73.66, 73.48, 39.23, 36.44, 33.95, 30.76, 27.31, 19.12 ppm. IR (KBr) ν_{max}: 2954, 2916, 2848, 2200, 1591, 1519, 1467, 1334, 1259, 1226, 1120, 846, 800, 570 cm^{-1}.

*5-(4-((3,4-Bis(hexadecyloxy)phenyl)ethynyl)phenyl)-2H-tetrazole (**4b**).* This was obtained in 90% yield as a colorless amorphous solid; mp: 115−116 °C. ^{1}H NMR (500 MHz, *d*-DMSO): δ 8.07−8.09 (d, J = 8 Hz, 2H), 7.64−7.66 (d, J = 8.0 Hz, 2H), 7.094−7.111 (d, J = 8.5 Hz, 1H), 7.05 (s, 1H), 6.89−6.90 (d, J = 8.0 Hz, 1H), 3.96−4.00 (t, 4H), 1.78−1.85 (m, 4H), 1.26−1.47 (m, 52H), 0.85−0.90 (t, 6H) ppm. ^{13}C NMR (125 MHz, *d*-DMSO): 154.95, 153.35, 137.19, 132.49, 130.59, 130.23, 121.45, 118.95, 118.62, 97.44, 92.29, 73.66, 73.48, 39.23, 36.44, 33.95, 30.76, 27.31, 19.12 ppm. IR (KBr) ν_{max}: 2954, 2916, 2848, 2200, 1591, 1519, 1467, 1334, 1259, 1226, 1120, 846, 800, 570 cm^{-1}.

*General Procedure for the Synthesis of **FD12** and **FD16**.* To a 250 mL two necked round-bottom flask kept under argon atmosphere was added 1,3,5-benzene tricarbonyl trichloride (1 equiv) dissolved in 10 mL of degassed pyridine. To this was added 5-(4-((3,4-Bis(alkoxy)phenyl)ethynyl)phenyl)-2*H*-tetrazole (3.6 equiv) dissolved in 30 mL of degassed pyridine dropwise using a pressure equalizer with constant stirring at room temperature for 15 min. The reaction mixture was then heated at 120 °C for 12 h. The reaction mixture was then poured into ice cold water, and the precipitate formed was then filtered, washed with water, and dried. The crude product was then purified by column chromatography by using silica gel (100−200 mesh) as the stationary phase and 30% EtOAc:hexane as the mobile phase.

*1,3,5-Tris(5-(4-((3,4-bis(dodecyloxy)phenyl)ethynyl)-phenyl)-1,3,4-oxadiazol-2-yl)benzene (**FD12**).* This was obtained in 75% yield; mp: 177 °C .^{1}H NMR (300 MHz, $CDCl_3$): δ 9.08 (s, 3H), 8.21−8.23 (d, J = 7.8 Hz, 6H), 7.73−7.71 (d, J = 7.8 Hz, 6H), 7.14−7.16 (d, J = 8.1 Hz), 7.08 (s, 3H), 6.84−6.87 (d, J = 8.1 Hz), 3.96−4.00 (t,4H), 1.78−1.85 (m, 4H), 1.26−1.47 (m, 36H), 0.85−0.90 (t, 6H) ppm. ^{13}C NMR (125 MHz, $CDCl_3$): 165.16, 162.79, 150.24, 148.79, 132.08, 127.86, 127.11, 126.19, 125.30, 122.15, 116.65, 114.50, 113.14, 93.48, 87.08, 69.30, 69.13, 31.94, 29.71, 29.65, 29.44, 29.38, 29.24, 29.19, 26.02, 22.70, 14.12 ppm. IR (KBr) ν_{max}: 2928, 2856, 2200, 1589, 1518, 1474, 1330, 1249, 1124, 1012, 844 cm^{-1}. MS (MALDI−TOF): calcd for $C_{126}H_{174}N_6O_9$ (M + H$^+$), 1917.77; found, 1917.64

*1,3,5-Tris(5-(4-((3,4-bis(hexadecyloxy)phenyl)ethynyl)-phenyl)-1,3,4-oxadiazol-2-yl)benzene (**FD16**).* This was obtained in 70% yiled; mp: 191 °C. ^{1}H NMR (300 MHz, $CDCl_3$): δ 9.08 (s, 3H), 8.21−8.23 (d, J = 7.8 Hz, 6H), 7.73−7.71 (d, J =

dx.doi.org/10.1021/jp305349h | J. Phys. Chem. B 2012, 116, 13071−13080

Scheme 1 [a]

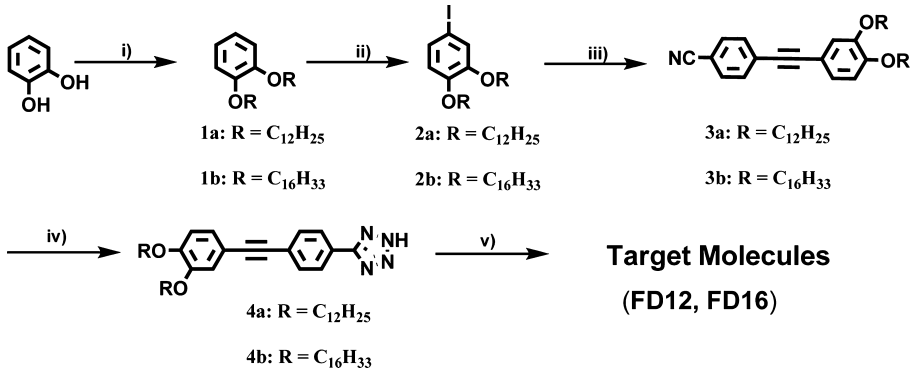

[a]Reagents and conditions: (i) R−Br, K_2CO_3, DMF, 80 °C, 24 h; (ii) *N*-iodosuccinimide, trifluoroacetic acid, ACN, room temperature, 6 h; (iii) 4-ethynylbenzonitrile, $Pd^{II}Cl_2$, CuI, PPh_3, THF, DIPA, room temperature, 12 h; (iv) NaN_3, NH_4Cl, DMF, 100 °C, 12 h; (v) 1,3,5-benzene tricarbonyl trichloride, pyridine, 120 °C, 12 h.

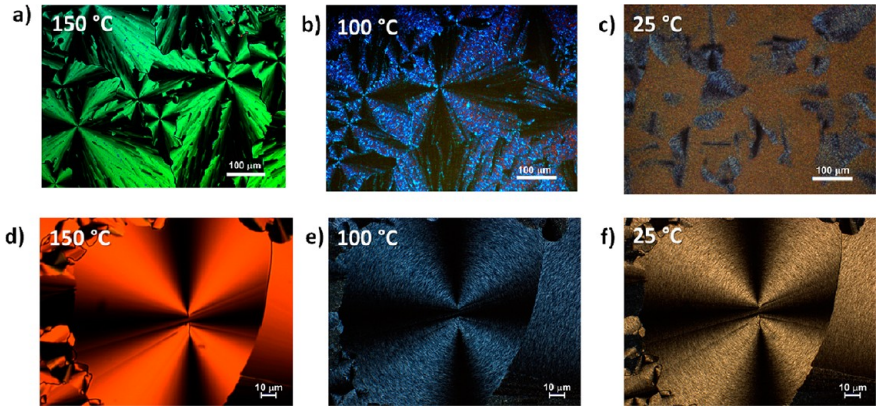

Figure 1. Polarized light optical microscopic (POM) images of **FD16** (top panel a, b, c) and **FD12** (bottom panel d, e, f).

7.8 Hz, 6H), 7.14−7.16 (d, *J* = 8.1 Hz), 7.08 (s, 3H), 6.84−6.87 (d, *J* = 8.1 Hz), 3.96−4.00 (t, 4H), 1.78−1.85 (m, 4H), 1.26−1.47 (m, 52H), 0.85−0.90 (t, 6H) ppm. ^{13}C NMR (125 MHz, $CDCl_3$): 165.16, 162.79, 150.24, 148.79, 132.08, 127.86, 127.11, 126.19, 125.30, 122.15, 116.65, 114.50, 113.14, 93.48, 87.08, 69.30, 69.13, 31.94, 29.71, 29.65, 29.44, 29.38, 29.24, 29.19, 26.02, 22.70, 14.12 ppm. IR (KBr) ν_{max}: 2922, 2851, 2204, 1595, 1512, 1467, 1330, 1249, 1124, 1012, 844 cm^{-1}. MS (MALDI−TOF): calcd for $C_{150}H_{222}N_6O_9$ ($M + H^+$), 2254.41; found, 2254.36

RESULTS AND DISCUSSION

Synthesis. Molecules **FD12** and **FD16** possessing C12 and C16 alkyl chain substituents, respectively, were synthesized according to Scheme 1.

The final reaction involved the conversion of tetrazole derivatives into oxadiazole derivatives by the Huisgen reaction mechanism.[11] All the intermediates as well as the final products were characterized using ^{1}H, ^{13}C NMR and IR spectroscopy.

Mesomorphic Properties. The mesomorphic properties of **FD12** and **FD16** were investigated by polarized light optical microscopy (POM) and differential scanning calorimetry (DSC). The DSC thermogram showed peaks at temperatures corresponding to those noted in the microscopic studies, confirming the phase transitions. POM images at various temperatures and the DSC thermogram of **FD12** and **FD16** are shown in Figures 1 and 2, respectively, and the phase transition temperatures and corresponding enthalpy values are summarized in Table 1. The first heating cycle of DSC was neglected to exclude the influences of thermal history of the samples. Both the derivatives were found to exhibit enantiotropic liquid crystalline mesophases over a wide range of temperature.

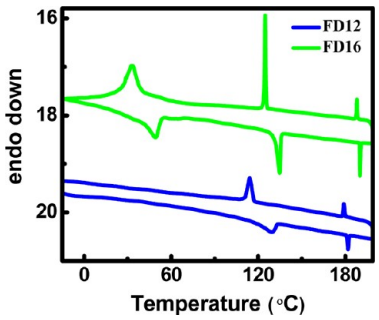

Figure 2. DSC thermogram of **FD16** and **FD12**.

In the first cooling cycle, **FD16** underwent an isotropic to liquid crystalline phase transition at 188 °C and the mesophase

Table 1. Phase Transition Temperature and Corresponding Thermodynamic Parameters of FD16 and FD12

	heating cycle [ΔH(kJ/mol)]	cooling cycle [ΔH(kJ/mol)]
FD16	Cr 49.4 °C (25.66) Col_{ob} 135 °C (16.18) Col_h190 °C (2.35) Iso	Iso 188 °C (2.24) Col_h 125 °C (17) Col_{ob}33.2 °C (26.32) Cr
FD12	Col_{ob} 129.2 °C (8.05) Col_h 182 °C (1.87) Iso	Iso 179 °C (1.7) Col_h 114.1 °C (10.37) Col_{ob}

dx.doi.org/10.1021/jp305349h | *J. Phys. Chem. B* 2012, 116, 13071−13080

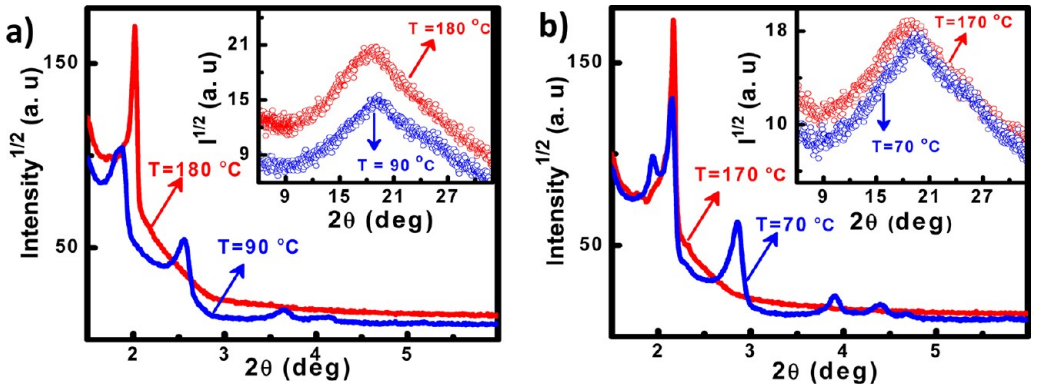

Figure 3. X-ray diffraction pattern of (a) **FD16** at 180 (red line) and 90 °C (blue line) and (b) **FD12** at 170 (red line) and 70 °C (blue line). Inset shows the corresponding XRD pattern obtained at higher 2θ region.

was assigned to hexagonal columnar mesophase based on the characteristic focal conic texture observed.[12,2a] Subsequent cooling resulted in the formation of striations on the arms of the focal conic texture at 125 °C. The appearance of striations on the arms of the focal conic texture are indicative of the formation of oblique columnar phase (Figure 1b).[12,2a] Further cooling resulted in the crystallization of **FD16** at 33 °C which is also clear from the appearance of an exothermic peak in the cooling cycle of DSC trace (Figure 2).

For **FD12** the first cooling cycle indicated an isotropic to hexagonal columnar mesophase transition at 179 °C. Similar to that observed for **FD16** further cooling resulted in the formation of striations on the arms of the focal conic texture (Figure 1e) indicating the formation of oblique columnar phase. Unlike for **FD16** however, the striated texture observed at higher temperatures was retained on cooling down to room temperature by which time the sample had solidified into a glass. POM image indicated that the liquid crystalline texture was retained in the glass (Figure 1f).[13] The formation of the glass was further confirmed from the absence of a clear crystallization peak in the cooling cycle in the DSC analysis (Figure 2).

The liquid crystalline mesophases were further confirmed using variable temperature X-ray diffraction (XRD) analysis (Figure 3).

The X-ray diffraction pattern of **FD16** at 180 °C showed a strong sharp peak at low angle (with a *d*-spacing of 43.76 Å) and broad and diffuse maxima in the wide angle region (with a spacing of 4.8 Å). Similarly for **FD12**, a strong sharp peak at low angle (with a *d*-spacing of 40.76 Å) and broad and diffuse maxima in the wide angle region (with a spacing of 4.7 Å) was observed at 170 °C. Owing to the presence of only one peak in the low angle region, the support of the POM texture is taken to label it as a hexagonal columnar phase, with a lattice spacing of 50.53 and 47.06 Å for **FD16** and **FD12** respectively. On further cooling the formation of striation on the arms of the focal conic texture was observed under POM at ~125 °C for **FD16** (at ~114 °C for **FD12**). The XRD measurements in this mesophase showed, for both the compounds, multiple peaks in the low angle region. The indexing of these peaks to a tilted columnar lattice was statistically slightly better than that to a rectangular columnar lattice; the tilt angle turns out to be ~3 degrees. The corresponding lattice parameters are tabulated in the Table 2.

Table 2. *d*-Spacing Values and Lattice Parameters of FD12 and FD16

sample	d_{meas} (Å)	d_{calc} (Å)	(*hk*)	lattice parameters	mesophase assigned
FD12	40.76	40.76	(10)	T = 170 °C	Col_h
	4.73			a = 47.06	
	44.75	44.88	(10)		Col_{Ob}
	41.29	41.24	(01)		
	31.15	31.08	(11)	T = 70 °C	
	22.66	22.44	(20)	a = 44.92 (Å)	
	20.15	20.10	(21)	b = 41.28 (Å)	
	18.86	19.07	(12)	γ = 2.6	
	4.58				
	3.47				
FD16	43.76			T = 180 °C	Col_h
	4.76			a = 50.53	
	48.53	48.48	(10)		Col_{Ob}
	46.83	46.87	(01)		
	34.65	34.46	(11)	T = 90 °C	
	24.28	24.24	(20)	a = 48.53 (Å)	
	21.54	21.92	(21)	b = 46.92 (Å)	
	4.65			γ = 2.5	
	3.51				

Gel Formation. The compounds **FD12** and **FD16** were found to aggregate strongly in nonpolar solvents such as decane even in the micro molar concentration range. On increasing the concentration beyond a threshold value (~10^{-2} M) formation of stable gels was observed. The gels were prepared by dissolving small amounts of the oxadiazole derivative in decane at higher temperature and allowing them to cool to room temperature in a closed vial. Gel formation was confirmed by the failure of the soft mass to flow by inverting the glass vial.[14] The critical gelation concentrations were found to be 15.6 mM and 13.3 mM for **FD12** and **FD16**, respectively. It must be mentioned here that the derivative **FD12** formed gel very slowly and it took several days (1−2 weeks) for complete immobilization of the solvent whereas **FD16** formed a gel within few minutes. Since the discotic molecules **FD12** and **FD16** do not possess any specific hydrogen bonding moieties, the self-assembly of these molecules would most likely occur through the combined effect of $\pi-\pi$ and dipole−dipole interactions. The microscopic structures of the self-assembled materials were investigated by scanning electron microscopy (SEM) and transmission electron microscopy (TEM) of these derivatives at 5 × 10^{-5} M concentration in decane. Figure 4 shows the SEM and TEM images observed for **FD16** (Figure

dx.doi.org/10.1021/jp305349h | *J. Phys. Chem. B* 2012, 116, 13071−13080

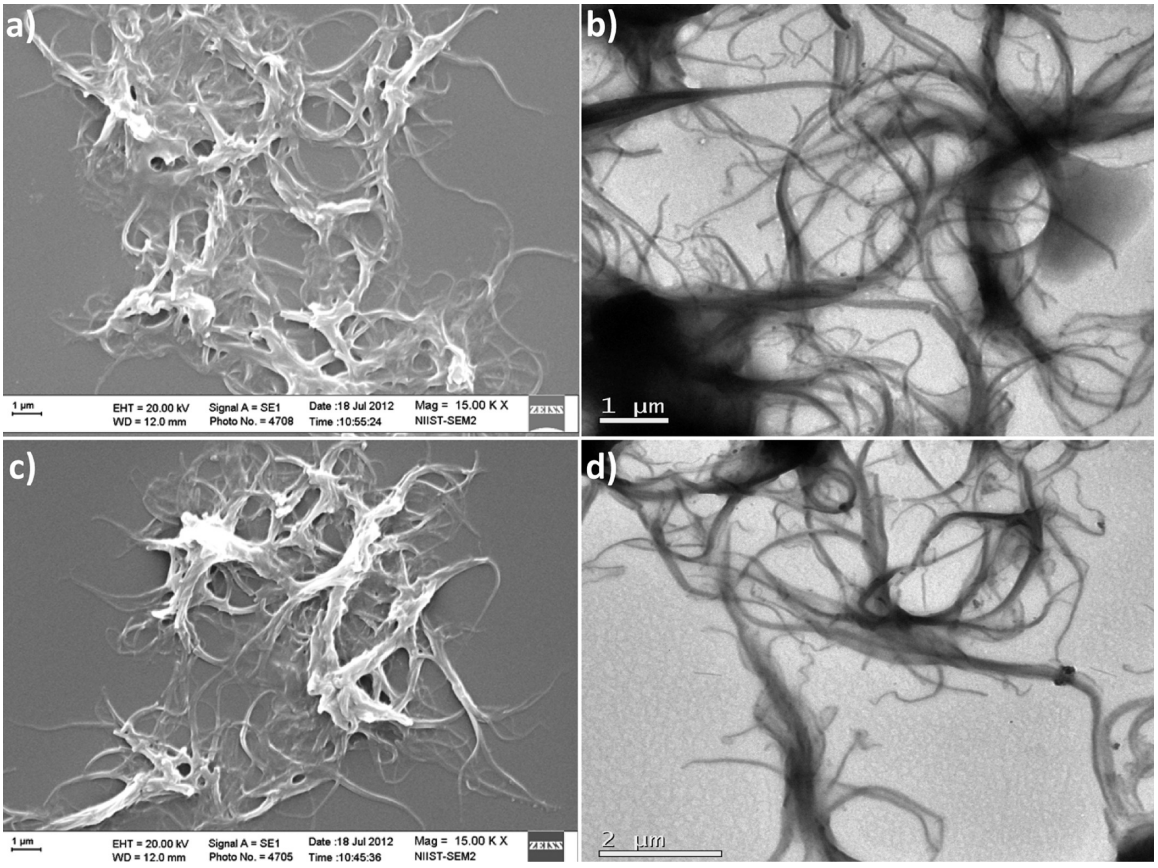

Figure 4. (a, b) SEM and TEM images of **FD16**; (c, d) SEM and TEM images of **FD12** (concentration 5 $\times 10^{-5}$ M in decane).

4a,b) and **FD12** (Figure 4c,d), which indicated a typical interlocked network structure of fibers.

In order to elucidate the molecular arrangements in the fibers we carried out X-ray diffraction studies (XRD) of both derivatives in their xerogel state. In the case of **FD16**, the XRD pattern showed intense peaks compared to its lower homologue in the higher 2θ regime (Figure 5), clearly

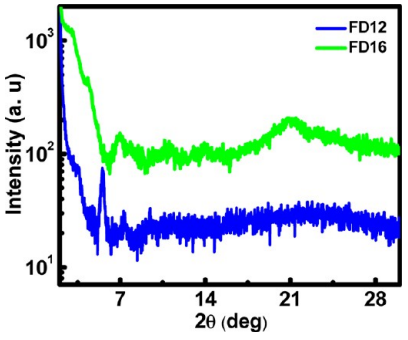

Figure 5. XRD pattern of **FD12** (blue line) and **FD16** (green line) in the xerogel state.

indicating the presence of much stronger $\pi-\pi$ interaction in the gel assemblies of **FD16** compared to that of **FD12**. Xerogel from **FD16** showed reflection peaks at 38.21, 23.76, 19.29, 11.98, and 4.15 Å. The reciprocal *d*-spacing ratio of these reflection peaks were identical to that obtained for oblique columnar arrangement (Col_{ob}) in liquid crystalline phase from variable temperature XRD analysis (Table 2). This clearly reveals the presence of oblique columnar arrangement in gel assemblies.[15] The same molecular arrangement was also observed for **FD12** xerogel from their XRD analysis.

Photophysical Properties. The photophysical properties of **FD12** and **FD16** were observed to be very sensitive to their state of aggregation. In solution the absorption spectra of these compounds were insensitive to solvent polarities. Their absorption spectra were however significantly broadened and red-shifted in the liquid crystalline and gel state compared to that in solution. The emission spectra showed significant broadening and red shift with increasing polarity of the solvent. In the liquid crystalline and gel state also the emission spectra were significantly broad and red-shifted comparable to that observed in the most polar solvent studied, namely benzonitrile. These aspects as well as detailed photophysical studies in the liquid crystalline and gel state have been investigated in detail.

(a). Solution State. Figure 6 shows the absorption and emission spectra of **FD12** in various solvents and the

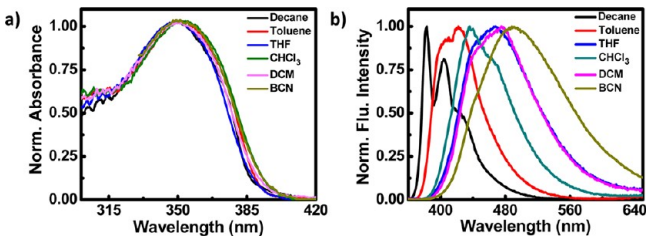

Figure 6. (a) Absorption and (b) emission spectra of **FD12** in different solvents.

dx.doi.org/10.1021/jp305349h | J. Phys. Chem. B 2012, 116, 13071−13080

absorption and emission data for both **FD12** and **FD16** are summarized in Table 3. The absorption spectra of both these

Table 3. Absorption, Emission, and Fluorescence Lifetime Characteristics of FD12 and FD16

		absorption	emission		
compound	solvent	λ_{max} (nm)	λ_{max} (nm)	Φ_F	τ (ns)
FD12	decane	349	382, 403, 430	0.66	0.83
	toluene	352	407, 421	0.75	0.99
	dichloromethane	350	477	0.77	2.33
	tetrahydrofuran	350	468	0.76	2.18
	benzonitrile	353	490	0.58	2.68
FD16	decane	350	382, 405, 432	0.68	0.87
	toluene	350	410, 419	0.77	1.01
	dichloromethane	350	477	0.75	2.31
	tetrahydrofuran	347	468	0.78	2.20
	benzonitrile	343	488	0.56	2.70

derivatives were found to be nearly identical, signifying that at the molecular level their optical properties were not affected by the length of the alkoxy substituent. Their absorption spectra were found to be fairly insensitive to solvent polarity (Figure 6a), which clearly indicates that the dipole moments of their ground and the corresponding Franck–Condon (FC) excited states are nearly the same. Their fluorescence spectra, however, showed a significant bathochromic shift with increasing polarity of the solvent (Figure 6b). In a weakly polar solvent like decane, the emission spectra exhibited sharp and structured emission bands whereas in polar solvents the emission spectra were broad and red-shifted.

The bathochromic shift in emission maximum and broadening of the band with solvent polarity point to the emissions arising from a charge transfer state, i.e., a state in which the dipole moments of the emissive state is significantly higher compared to that of their ground state. This can occur when excitation of these molecules leads to a nonemissive locally excited state (LE) of nearly same dipole moment as the ground state, which then subsequently transforms into a more polar emissive state via intramolecular charge transfer (ICT) process.[16] The existence of dual excited states has been reported in several donor–acceptor molecules[17] including stilbene[18] and butadiene derivatives.[19]

(b). Liquid Crystalline State. The excitation and emission properties of the liquid crystalline phases of **FD12** and **FD16** were investigated in the reflection mode using thin films maintained at controlled temperatures, by initially heating the materials to their isotropic phase and slowly cooling them to the desired temperatures. The emission and excitation spectra for **FD16** and **FD12** films at the various temperatures are shown in Figures 7 and 8, respectively.

The emission spectra were broad for both the derivatives, and an increase in temperatures led to a reduction in the emission intensity without any significant change in the spectral shape. Interestingly, both the materials exhibit appreciable fluorescence even at the higher temperatures required to generate the isotropic form. Cooling of the isotropic phase to the columnar liquid crystalline phase resulted in an increase in the fluorescence intensity and a further increase in intensity was observed on solidification. The glass formed by **FD12** on cooling, was highly transparent as shown in the Figure 9a and

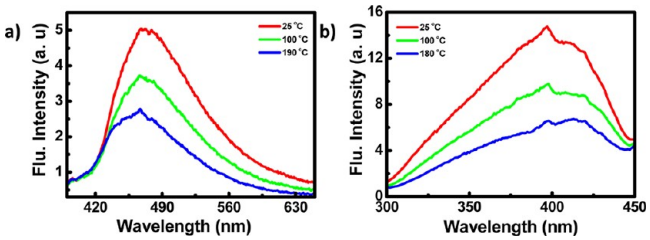

Figure 7. Temperature dependent changes on (a) emission spectra ($\lambda_{exc.}$= 350 nm) and (b) excitation spectra (emission collected at 475 nm) of **FD16**.

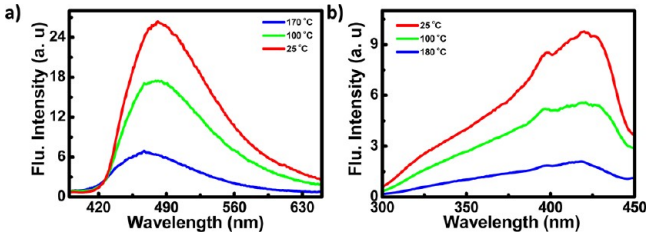

Figure 8. Temperature dependent changes on (a) emission spectra ($\lambda_{exc.}$= 350 nm) and (b) excitation spectra (emission collected at 475 nm) of **FD12**.

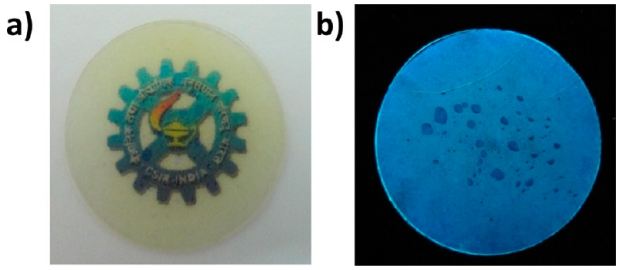

Figure 9. Photograph of **FD12** in the liquid crystalline glassy state under (a) ordinary light and (b) 365 nm UV illuminations.

was observed to be stable over a period of 1 year. The glassy film of **FD12** exhibited blue emission (λ_{max} = 475 nm; Figure 9b) with an absolute quantum yield of 26%. The crystalline film formed by cooling **FD16** also exhibited blue luminescence (λ_{max} = 472 nm) although with a significantly lower absolute quantum yield of 9%. The broad emission band combined with the significant red shift in the maxima of the excitation spectra of these films compared to their absorption spectra in solution are indicative of the emission arising from the aggregated state of these molecules in the solid, liquid crystalline as well as isotropic phases.

(c). Aggregated and Gel State. As discussed earlier, **FD12** and **FD16** had a strong tendency to form aggregates in nonpolar solvents, forming gels in decane at concentrations greater than 15.6 mM and 13.3 mM, respectively. Since the aggregation process for these materials in solvents was a slow process, and since aggregation was also observed to lead to significant differences in their photophysical properties, we have investigated the time dependent changes in the UV–vis absorption of these derivatives. With time, a reduction in the intensity of the peak observed at the short wavelength with a maxima centered on 350 nm, attributable to the monomer peak by comparison with the absorption spectra obtained in solutions (Figure 6a), was observed and this change was accompanied by an increase in intensity in the longer

dx.doi.org/10.1021/jp305349h | J. Phys. Chem. B 2012, 116, 13071–13080

wavelength region was observed. For **FD16**, the increase in intensity in the long wavelength was much clearer and a distinct shoulder band at 400 nm could also be observed (Figure 10a).

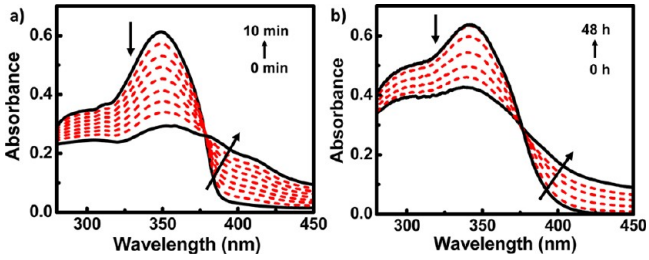

Figure 10. Time dependent changes in absorption spectra of (a) **FD16** (10^{-5} M; 1 cm ×1 cm) and (b) **FD12** (10^{-5} M) in decane.

This change was completed by about 10 min. For **FD12** however, the decrease in intensity of monomer peak with time was much slower, taking about 48 h for completion, and only a broadening of the band could be observed (Figure 10b). These results clearly show that the tendency to form closely packed exciton coupled aggregates is much stronger for **FD16** than for **FD12**.

The time dependent formation of aggregates can be clearly visualized by subtracting the contribution of the monomer band (obtained from the absorption spectrum measured at zero time where molecule exists mainly in the molecularly dissolved state) from the absorption spectrum obtained at the end of measurements (10 min for **FD16** and 48 h for **FD12**) following normalization at 347 nm (Figure 11).

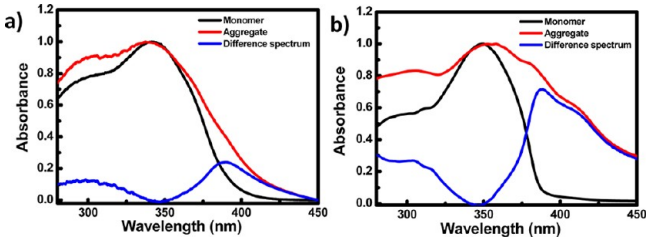

Figure 11. Difference spectra (blueline) of (a) **FD12** and (b) **FD16** obtained by subtracting the absorption spectrum of monomer (black line) from absorption spectrum of completely aggregated solution (red line).

The difference spectra obtained for both derivatives showed two peaks, one blue-shifted and the other red-shifted compared to the monomer absorption band. For both derivatives the intensity of blue-shifted band are comparable whereas the contribution of red-shifted aggregate is significantly higher for **FD16** compared to **FD12**, indicating an increased propensity for **FD16** to form red-shifted aggregates.

Aggregate formation in these molecules was observed to be sensitive to the temperature of the solution. Figure 12 shows the absorption spectrum of both the derivatives as a function of temperature from 20 to 70 °C with an increment of 5 °C. An increase in temperature leads to a reduction in the intensity of absorption in the long wavelength region and a concomitant increase in the intensity of absorption in the lower wavelength region attributable to the monomer absorption was observed. Unlike in the case of **FD12**, the breakup of aggregates to monomer species was not complete in **FD16** even at higher

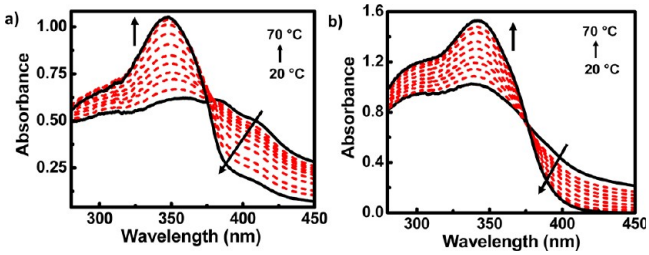

Figure 12. Effect of temperature on absorption spectra of (a) **FD16** (1.5×10^{-5} M; 1 cm ×1 cm) and (b) **FD12** (1.5×10^{-5} M) in decane.

temperatures (Figure 12a). This clearly indicates that aggregates formed in **FD16** were much stronger.

The fraction of aggregate at each temperature ($\alpha_{agg}(T)$) was estimated using the following equation:

$$\alpha_{agg}(T) \approx \frac{A(T) - A_{mono}}{A_{agg} - A_{mono}}$$

Here $\alpha_{agg}(T)$ is the fraction of aggregate at temperature T, and A_{mono}, $A(T)$, and A_{agg} are the absorbance at 347 nm for the monomer, the solution at temperature T, and the pure aggregate solutions, respectively.[20] The $\alpha_{agg}(T)$ values were then plotted as a function of temperature and from such a plot the $\alpha_{50}(T)$ (temperature at which α_{agg} = 0.5) was calculated (Figure 13).

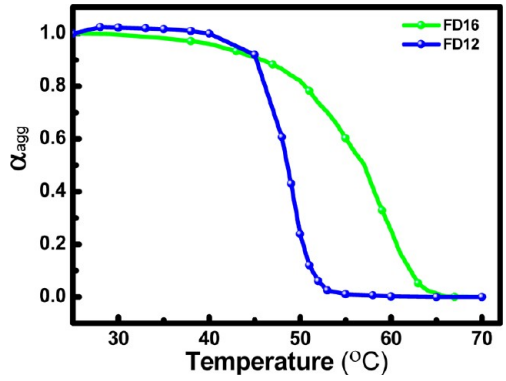

Figure 13. Plot of fraction of aggregate (α_{agg}) as a function of temperature (1.5×10^{-5} M) for **FD12** (blue line) and **FD16** (green line).

The melting of the stacks in **FD12** takes place in a relatively narrow temperature range (~10 °C) indicating that the thermal stability of the stacks is relatively weak compared to **FD16** (temperature range ~20 °C). The $\alpha_{50}(T)$ values obtained for **FD16** and **FD12** are 57 and 48.5 °C respectively. The lower $\alpha_{50}(T)$ value for **FD12** compared to **FD16** indicates that the latter derivative forms stronger aggregates.

The breakup of the aggregates at higher temperatures into their monomer form was also indicated by the changes in their fluorescence behavior. For **FD16**, with increase in temperature the intensity of aggregate band at 480 nm in the emission spectrum decreased and that at 382 nm attributable to the monomer peak increased (Figure 14a). For **FD12** however only a general increase in intensity of main emission band with increasing temperature was observed (Figure 14b). The temperature dependent excitation spectra of both derivatives in their aggregated solutions (2×10^{-5} M) also showed significant differences. In the case of **FD16**, the solution at

dx.doi.org/10.1021/jp305349h | J. Phys. Chem. B 2012, 116, 13071−13080

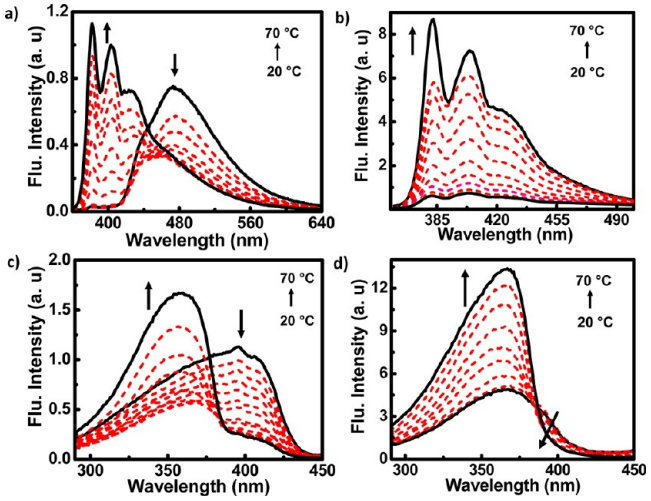

Figure 14. Temperature dependent changes in emission spectra (λ_{ex} = 350 nm) of (a) **FD16** (1.5×10^{-5} M; 1 cm × 1 cm) and (b) **FD12** (1.5×10^{-5} M) in decane. Effect of temperature on excitation spectra of (c) **FD16** (2×10^{-5} M; λ_{em} = 470 nm) and (d) **FD12** (2×10^{-5} M; λ_{em} = 470 nm) in decane.

lower temperature showed an excitation maximum at 400 nm whereas monomer had an excitation maximum centered at 360 nm, indicating the nature of the excited species to be clearly different, namely the aggregate (Figure 14c). The band at 400 nm coincides with the absorption spectrum of aggregated solution (Figure 10a). Here also the excitation spectrum at higher temperature shows contributions from the aggregate which is evident from the shoulder at 400 nm, indicating the aggregate formed is much stronger for **FD16**. However, in the case of **FD12**, there was no considerable change in the excitation maximum with temperature (Figure 14d).

The differences in photophysical properties between the aggregated state of **FD12** and **FD16** were even more prominent in their gels. The **FD12** gel absorption peak obtained from its reflectance spectra was significantly blue-shifted compared that of the **FD16** gel and this difference could be visually perceived, with the **FD12** gel being nearly colorless, and the **FD16** gel exhibiting a pale green color (Figure 15a).

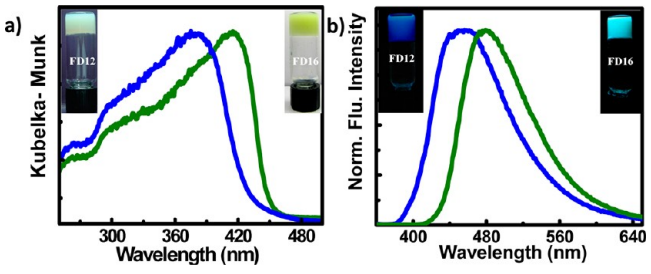

Figure 15. (a) Absorption and (b) emission spectra of **FD12** (blue line), **FD16** (green line) in gel (λ_{ex} = 350 nm; 2×10^{-2} M in decane; 1 mm cuvette). Inset shows the corresponding photographs of gel under white light and 365 nm UV illumination.

The gels derived from **FD12** exhibited blue emission with the (λ_{max}= 450 nm) whereas the gel from **FD16** exhibited bluish green emission (λ_{max}= 480 nm, Figure 15b). The absolute quantum yields of these gels were determined to be 11% and 6% for **FD12** and **FD16** respectively.

On the basis of these studies, it is clear that **FD16** molecules has higher tendency for formation of strongly exciton coupled aggregates compared to **FD12**. The large red-shift in absorption and emission spectra especially for **FD16** in its condensed phases as well as in solutions at higher concentrations as well their strong dependence on temperature clearly shows that these effects arise due to aggregation of the molecules. Aggregation of molecules in the ground state can result in exciton coupling as described by Kasha et al., in which the excited state of aggregates splits into two energy levels (Davydov splitting).[21] The transition to the upper state is allowed in the case of molecules with cofacial arrangements (H-aggregates), and this is characterized by a hypsochromically shifted absorption band compared to that of the monomer, whereas transition to the lower state is allowed for aggregates arranged in a slipped stack or a head-to-tail fashion (J-aggregates) resulting in a bathochromically shifted absorption band compared to the isolated monomer. Although the derivatives investigated in the present study form both blue and red-shifted aggregates indicating the formation of both H-type and J-type aggregates, exciton coupling was much stronger for **FD16** indicating that its molecules are much more closely packed in the aggregated state.

CONCLUSION

Two discotic molecules **FD16** and **FD12**, based on the 1,3,4-oxadiazole moiety have been synthesized and characterized. Both derivatives exhibited enantiotropic columnar mesophases over a wide range of temperature. **FD12** with C12 alkyl chain transforms upon cooling from isotropic state to a glassy film at room temperature wherein the liquid crystalline order is maintained. The glassy film formed was highly transparent and stable and was found to show blue luminescence with an absolute quantum yield of 26%. The columnar liquid crystalline ordering along with a fairly good blue emission in the glassy state of **FD12** could make this material applicable for nondoped blue emitting diodes and display devices. Both the derivatives form stable luminescent gels in decane, wherein the molecules are arranged in an oblique columnar fashion as evident from their XRD measurements. The optical properties of these derivatives in gel state were found to be alkyl chain dependent. The gel derived from **FD12** exhibited blue emission whereas **FD16** exhibited bluish-green emission in decane. The self-assembling processes were studied in detail using time and temperature dependent UV−vis absorption and emission measurements. The extent of aggregation was found to be higher in **FD16** which is evident from their large red shift observed in absorption and emission spectra compared to the other derivative. These observations clearly demonstrate that perturbation of molecular structure has remarkable influence on their bulk macroscopic properties. These effects exemplify the future possibilities of fine-tuning the optical properties of molecules in soft organic materials.

AUTHOR INFORMATION

Corresponding Author

*Fax: (+91) 471-2490186. E-mail: sureshdas@niist.res.in.

Notes

The authors declare no competing financial interest.

■ ACKNOWLEDGMENTS

This work is supported by Council of Scientific and Industrial Research (CSIR) under the Project NWP 55. D.D.P, N.S.S.K, A.P.S., and S.V. are grateful to CSIR for fellowships. This is Contribution No. NIIST-PPG-329. The authors thank Dr. S. Krishna Prasad and Dr. D. S. Shankar Rao, CSMR Bangalore, for carrying out variable temperature XRD measurements and discussions.

■ REFERENCES

(1) (a) Sergeyev, S.; Pisula, W.; Geerts, Y. H. *Chem. Soc. Rev.* **2007**, *36*, 1902−1929. (b) Pisula, W.; Feng, X.; Müllen, K. *Chem. Mater.* **2011**, *23*, 554−567. (c) Laschat, S.; Baro, A.; Steinke, N.; Giesselmann, F.; Hägele, C.; Scalia, G.; Judele, R.; Kapatsina, E.; Sauer, S.; Schreivogel, A.; Tosoni, M. *Angew. Chem., Int. Ed.* **2007**, *46*, 4832−4887.

(2) (a) Varghese, S.; Kumar, N. S. S.; Krishna, A.; Rao, D. S. S.; Prasad, S. K.; Das, S. *Adv. Funct. Mater.* **2009**, *19*, 2064−2073. (b) Kaafarani, B. R. *Chem. Mater.* **2011**, *23*, 378−396. (c) Shimizu, Y.; Oikawa, K.; Nakayamac, K.-I.; Guillon, D. *J. Mater. Chem.* **2007**, *17*, 4223−4229. (d) Schmidt-Mende, L.; Fechtenkötter, A.; Müllen, K.; Moons, E.; Friend, R. H.; MacKenzie, J. D. *Science* **2001**, *293*, 1119−1122. (e) Yasuda, T.; Shimizu, T.; Liu, F.; Ungar, G.; Kato, T. *J. Am. Chem. Soc.* **2011**, *133*, 13437−13444. (f) An, Z.; Yu, J.; Domercq, B.; Jones, S. C.; Barlow, S.; Kippelen, B.; Marder, S. R. *J. Mater. Chem.* **2009**, *19*, 6688−6698. (g) Adam, D.; Schumacher, P.; Simmerer, J.; Häussling, L.; Siemensmeyer, K.; Etzbach, K. H.; Ringsdorf, H.; Haarer, D. *Nature* **1994**, *371*, 141−143.

(3) (a) Christ, T.; Stümpflen, V.; Wendorff, J. H. *Macromol. Rapid Commun.* **1997**, *18*, 93−98. (b) Seguy, I.; Destruel, P.; Bock, H. *Synth. Met.* **2000**, *111*, 15−18. (c) Christ, T.; Glüsen, B.; Greiner, A.; Kettner, A.; Sander, R.; Stümpflen, V.; Tsukruk, V.; Wendorff, J. H. *Adv. Mater.* **1997**, *9*, 48−52. (d) Lüssem, G.; Wendorff, J. H. *Polym. Adv. Technol.* **1998**, *9*, 443−460. (e) Hassheider, T.; Benning, S. A.; Kitzerow, H. S.; Achard, M. F.; Bock, H. *Angew. Chem., Int. Ed.* **2001**, *40*, 2060−2063. (f) Alibert-Fouet, S.; Dardel, S.; Bock, H.; Oukachmih, M.; Archambeau, S.; Seguy, I.; Jolinat, P.; Destruel, P. *ChemPhysChem.* **2003**, *4*, 983−985. (g) Bacher, A.; Bleyl, I.; Erdelen, C. H.; Haarer, D.; Paulus, W.; Schmidt, H.-W. *Adv. Mater.* **1997**, *9*, 1031−1035.

(4) (a) Varghese, S.; Das, S. *J. Phys. Chem. Lett.* **2011**, *2*, 863−873. (b) Das, S.; Varghese, S.; Kumar, N. S. S. *Langmuir* **2010**, *26*, 1598−1609. (c) Kumar, N. S. S.; Varghese, S.; Suresh, C. H.; Rath, N. P.; Das, S. *J. Phys. Chem. C* **2009**, *113*, 11927−11935. (d) Davis, R.; Kumar, N. S. S.; Abraham, S.; Suresh, C. H.; Rath, N. P.; Tamaoki, N.; Das, S. *J. Phys. Chem. C* **2008**, *112*, 2137−2146. (e) Kumar, N. S. S.; Varghese, S.; Rath, N. P.; Das, S. *J. Phys. Chem. C* **2008**, *112*, 8429−8437. (f) Kumar, N. S. S.; Varghese, S.; Narayan, G.; Das, S. *Angew. Chem., Int. Ed.* **2006**, *118*, 6465−6469.

(5) (a) Birks, J. B., *Photophysics of Aromatic Molecules*; Wiley: London, 1970. 704. (b) Cornil, J.; Beljonne, D.; Calbert, J-P.; Brédas, J.-L. *Adv. Mater.* **2001**, *13*, 1053−1067. (c) Kim, J.; Swager, T. M. *Nature* **2001**, *411*, 1030−1034.

(6) Hayer, A.; de Halleux, V.; Köhler, A.; El-Garoughy, A.; Meijer, E. W.; Barberà, J.; Tant, J.; Levin, J.; Lehmann, M.; Gierschner, J.; Cornil, J.; Geerts, Y. H. *J. Phys. Chem. B* **2006**, *110*, 7653−7659.

(7) Cristiano, R.; Gallardo, H.; Bortoluzzi, A. J.; Bechtold, I. H.; Campos, C. E. M.; Longo, R. L. *Chem. Commun.* **2008**, 5134−5136.

(8) (a) Hughes, G.; Bryce, M. R. *J. Mater. Chem.* **2005**, *15*, 94−107. (b) Zhang, Y.-D.; Jespersen, K. G.; Kempe, M.; Kornfield, J. A.; Barlow, S.; Kippelen, B.; Marder, S. R. *Langmuir* **2003**, *19*, 6534−6536. (c) Tamoto, N.; Adachi, C.; Nagai, K. *Chem. Mater.* **1997**, *9*, 1077−1085. (d) Tang, J.; Huang, R.; Gao, H.; Cheng, X.; Prehm, M.; Tschierske, C. *RSC Adv.* **2012**, *2*, 2842−2847. (e) Qu, S.; Wang, L.; Liu, X.; Li, M. *Chem.—Eur. J.* **2011**, *17*, 3512−3518. (f) Wanga, H.; Zhanga, F.; Baia, B.; Zhanga, P.; Shia, J.; Yub, D.; Zhaob, Y.; Wang, Y.; Li, M. *Liq. Cryst.* **2008**, *35*, 905−912. (g) Ryu, S. Y.; Kim, S.; Seo, J.; Kim, Y.-W.; Kwon, O.-H.; Jang, D.-J.; Park, S. Y. *Chem. Commun.* **2004**, 70−71. (h) Qu, S.; Wang, H.; Zhu, W.; Luo, J.; Fan, Y.; Song, L.; Zhang, H.-X.; Liu, X. *J. Mater. Chem.* **2012**, *22*, 3875−3881.

(9) (a) Cho, I.; Kim, S. H.; Kim, J. H.; Park, S.; Park, S. Y. *J. Mater. Chem.* **2012**, *22*, 123−129. (b) Chen, Y.-H.; Lin, S. L.; Chang, Y. C.; Chen, Y. C.; Lin, J. T.; Lee, R. H.; Kuo, W. J.; Jeng, R. J. *Org. Electron* **2012**, *13*, 43−52. (c) Zheng, C. J.; Zhao, W. M.; Wang, Z. Q.; Huang, D.; Ye, J.; Ou, X. M.; Zhang, X. H.; Lee, C. S.; Lee, S. T. *J. Mater. Chem.* **2010**, *20*, 1560−1566. (d) Wang, Z. Q.; Xu, C.; Wang, W. Z.; Duan, L.; Li, M. Z.; Zhao, B. T.; Ji, B. M. *New. J. Chem.* **2012**, *36*, 662−667. (e) Kim, S. H.; Cho, I.; Sim, M. K.; Park, S.; Park, S. Y. *J. Mater. Chem.* **2011**, *21*, 9139−9148. (f) Thangthong, A. M.; Prachumrak, N.; Tarsang, R.; Keawin, T.; Jungsuttiwong, S.; Sudyoadsuk, T.; Promarak, V. *J. Mater. Chem.* **2012**, *22*, 6869−6877.

(10) Prasad, S. K.; Rao, D. S. S.; Sridevi, S.; Lobo, C. V.; Ratna, B. R.; Naciri, J.; Shashidhar, R. *Phys. Rev. Lett.* **2009**, *102*, 147802(1−4).

(11) (a) Reddy, M. A.; Malleshama, G.; Thomas, A.; Srinivas, K.; Rao, V. J.; Bhanuprakash, K.; Giribabu, L.; Grover, R.; Kumar, A.; Kamalasanan, M. N.; Srivastava, R. *Synth. Met.* **2011**, *161*, 869−880. (b) Verheyde, B.; Dehaen, W. *J. Org. Chem.* **2001**, *66*, 4062−4064. (c) Bettenhausen, J.; Strohriegl, P. *Adv. Mater.* **1996**, *8*, 507−510.

(12) Dierking, I., *Textures of Liquid Crystals*, Ed., Wiley-VCH: Weinheim, Germany, 2003.

(13) (a) Wu, J.; Usui, T.; Hanna, J. *J. Mater. Chem.* **2011**, *21*, 8045−8051. (b) Abraham, S.; Mallia, V. A.; Ratheesh, K. V.; Tamaoki, N.; Das, S. *J. Am. Chem. Soc.* **2006**, *128*, 7692−7698. (c) Mallia, V. A.; Tamaoki, N. *Chem. Soc. Rev.* **2004**, *33*, 76−84. (d) Glüsen, B.; Kettner, A.; Kopitzke, J.; Wendorff, J. H. *J. Non-Cryst. Solids* **1998**, *241*, 113−120.

(14) (a) George, M.; Weiss, R. G. *Langmuir* **2002**, *18*, 7124. (b) Murata, K.; Aoki, M.; Suzuki, T.; Harada, T.; Kawabata, H.; Komori, T.; Ohseto, F.; Ueda, K.; Shinkai, S. *J. Am. Chem. Soc.* **1994**, *116*, 6664−6676.

(15) (a) Bai, B.; Wang, H.; Xin, H.; Zhang, F.; Long, B.; Zhang, X.; Qu, S.; Li, M. *New J. Chem.* **2007**, *31*, 401−408. (b) Shirakawa, M.; Fujita, N.; Tani, T.; Kaneko, K.; Shinkai, S. *Chem. Commun.* **2005**, 4149−4151. (c) Hashimoto, M.; Ujiie, S.; Mori, A. *Adv. Mater.* **2003**, *15*, 797−800.

(16) (a) Demeter, A.; Druzhinin, S.; George, M.; Haselbach, E.; Roulin, J.-L.; Zachariasse, K. A. *Chem. Phys. Lett.* **2000**, *323*, 351. (b) Rettig, W. *Electron Transfer 1*; Mattey, J., Ed.; Topics of Current Chemistry 169; Springer: Berlin, 1994; p 253.

(17) (a) Galievsky, V. A.; Druzhinin, S. I.; Demeter, A.; Kovalenko, S. A.; Senyushkina, T.; Mayer, P.; Zachariasse, K. A. *J. Phys. Chem. A* **2011**, *115*, 10823−10845. (b) Zachariasse, K. A.; Druzhinin, S. I.; Bosch, W.; Machinek, R. *J. Am. Chem. Soc.* **2004**, *126*, 1705−1715. (c) Schuddeboom, W.; Jonker, S. A.; Warman, J. M.; Leinhos, U.; Kuehnle, W.; Zachariasse, K. A. *J. Phys. Chem.* **1992**, *96*, 10809−10819.

(18) (a) Singh, A. K.; Kanvah, S. *J. Chem. Soc., Perkin Trans.* **2001**, *2*, 395−401. (b) Gilabert, E.; Lapouyade, R.; Rulliere, C. *Chem. Phys. Lett.* **1991**, *185*, 82.

(19) (a) Davis, R.; Das, S.; George, M. V.; Druzhinin, S.; Zachariasse, K. A. *J. Phys. Chem. A* **2001**, *105*, 4790. (b) Singh, A. K.; Manjula, D.; Kanvah, S. *New. J. Chem.* **1999**, *23*, 1075. (c) Singh, A. K.; Manjula, D.; Kanvah, S. *J. Phys. Chem.* **2000**, *104*, 464.

(20) Ghosh, S.; Li, X.-Q.; Stepanenko, V.; Würthner, F. *Chem.—Eur. J.* **2008**, *14*, 11343.

(21) (a) Würthner, F.; Kaiser, T. E.; Saha-Möller, C. R. *Angew. Chem., Int. Ed.* **2011**, *50*, 3376−3410. (b) Kasha, M.; Rawls, H. R.; El-Bayoumi, M. A. *Pure Appl. Chem.* **1965**, *11*, 371. (c) Davydov, A. S. *Theory of Molecular Excitons*; Plenum Press: New York, 1971.